Test beam evaluation of newly developed n-in-p planar pixel sensors for use in a high radiation environment

K. Kimura [v,*], D. Yamaguchi [v], K. Motohashi [v], K. Nakamura [n], Y. Unno [n], O. Jinnouchi [v], S. Altenheiner [b], A. Blue [c], M. Bomben [f,k,l], A. Butter [e,f,g], A. Cervelli [a], S. Crawley [c], A. Ducourthial [f,k,l], A. Gisen [b], M. Hagihara [w], K. Hanagaki [t,n], K. Hara [w,x], M. Hirose [v], Y. Homma [v], Y. Ikegami [n], S. Kamada [m], T. Kono [s], A. Macchiolo [r], G. Marchiori [f,k,l], F. Meloni [a], M. Milovanovic [j], A. Morton [c], G. Mullier [a], F.J. Munoz [q], C. Nellist [e,f,g], B. Paschen [r,1], A. Quadt [d], T. Rashid [e,f,g], J. Rieger [d], A. Rummler [f,h,i], K. Sato [w], K. Sato [w,x], N. Savic [r], H. Sawai [v], K. Sexton [c], M.E. Stramaglia [a], M. Swiatlowski [u], R. Takashima [o], Y. Takubo [n], S. Terzo [r], K. Todome [v], J. Tojo [p], K. Van Houten [u], J. Weingarten [d], S. Wonsak [j], K. Wraight [c], K. Yamamura [m]

[a] Universität Bern, Laboratory for High Energy Physics, Sidlerstrasse 55, CH-3012 Bern, Switzerland
[b] Experimentelle Physik IV, Technische Universität Dortmund, 44221 Dortmund, Germany
[c] School of Physics and Astronomy, University of Glasgow, Glasgow, G12 8QQ, Scotland, United Kingdom
[d] Georg-August-Universität Göttingen, Friedrich-Hund-Platz 1, D-37081 Göttingen, Germany
[e] LAL, University Paris-Sud, France
[f] CNRS/IN2P3, France
[g] Université Paris-Saclay, Orsay, France
[h] LAPP, France
[i] Université Savoie Mont Blanc, Annecy-le-Vieux, France
[j] Department of Physics, University of Liverpool, Merseyside, Liverpool, L69 3BX, United Kingdom
[k] Laboratoire de physique nucléaire et de hautes energies (LPNHE), Univ. Paris-UMPC, 4 Place Jussieu, 75005 Paris, France
[l] Univ. Paris Diderot, France
[m] Solid State Div., Hamamatsu Photonics K.K., 1126-1, Ichino-cho, Higashi-ku, Hamamatsu-shi, Shizuoka 435-8558, Japan
[n] Institute of Particle and Nuclear Study, KEK, Oho 1-1, Tsukuba, Ibaraki 305-0801, Japan
[o] Department of Science Education, Kyoto University of Education, Kyoto 612-8522, Japan
[p] Department of Physics, Faculty of Science, Kyushu University 744 Motooka, Nishi-ku, Fukuoka 819-0395, Japan
[q] School of Physics and Astronomy, University of Manchester, Oxford Road, Manchester M13 9PL, United Kingdom
[r] Max-Planck-Institut für Physik, Föhringer Ring 6, D-80805 München, Germany
[s] Ochadai Academic Production, Ochanomizu University, 2-1-1, Otsuka, Bunkyo-ku, Tokyo, 112-8610, Japan
[t] Department of Physics, Osaka University, Machikaneyama-cho 1-1, Toyonaka-shi, Osaka 560-0043, Japan
[u] SLAC National Accelerator Laboratory, 2575 Sand Hill Road, Menlo Park, CA 94025, United States of America
[v] Institute of Science and Engineering, Tokyo Institute of Technology, Ookayama 2-12-1, Meguro-ku, Tokyo 152-8551, Japan
[w] Institute of Pure and Applied Sciences, University of Tsukuba, Tsukuba, Ibaraki 305-8751, Japan
[x] Center for Integrated Research in Fundamental Science and Engineering, University of Tsukuba, Tsukuba, Ibaraki 305-8571 Japan

ARTICLE INFO

ABSTRACT

Radiation-tolerant n-in-p planar pixel sensors have been under development in cooperation with Hamamatsu Photonics K.K. (HPK). This is geared towards applications in high-radiation environments, such as for the future Inner Tracker (ITk) placed in the innermost part of the ATLAS detector in the high luminosity LHC (HL-LHC) experiment. Prototypes of those sensors have been produced, irradiated, and evaluated over the last few years. In the previous studies, it was reported that significant drops in the detection efficiency were observed after irradiation, especially under bias structures. The bias structures are made up of poly-Si or Al bias rails and poly-Si bias resistors. The structure is implemented on the sensors to allow quality checks to be performed before the bump-bonding process, and to ensure that charge generated in floating pixels due to non-contacting or missing bump-bonds is dumped in a

Bulk damage
Surface damage
Bias structure

controlled way in order to avoid noise. To minimize the efficiency drop, several new pixel structures have been designed with bias rails and bias resistors relocated. Several test beams have been carried out to evaluate the drops in the detection efficiency of the new sensor structures after irradiation. Newly developed sensor modules were irradiated with proton-beams at the Cyclotron and Radio-Isotope Center (CYRIC) in Tohoku University to see the effect of sensor-bulk damage and surface charge-up. An irradiation with γ-rays was also carried out at Takasaki Advanced Radiation Research Center, with the goal of decoupling the effect of surface charge-up from that of bulk damage. Those irradiated sensors have been evaluated with particle beams at DESY and CERN. Comparison between different sensor structures confirmed significant improvements in minimizing efficiency loss under the bias structures after irradiation. The results from γ-irradiation also enabled cross-checking the results of a semiconductor technology simulation program (TCAD).

1. Introduction

A new pixel sensor has been developed by Hamamatsu Photonics K.K. (HPK) [1] in collaboration with the ATLAS Japan Silicon Group [2–4]. R&D for this pixel sensor is geared towards applications in High Energy Physics experiments, such as for the future Inner Trackers (ITk) of the ATLAS detector in the high luminosity LHC (HL-LHC) experiment [5]. Since the pixel detectors have been developed with the aim of tracking short-lived charged particles, they are usually installed in the inner-most part of particle detectors. Thus, they are required to have high radiation-tolerance, such as 1.0×10^{16} n_{eq}/cm^2 for the inner layers, and 1.7×10^{15} n_{eq}/cm^2 for the outer layers of ITk in HL-LHC for instance [5]. In order to achieve this requirement, new pixel detectors have adopted n-in-p type silicon structure. It was reported that both n-in-p and n-in-n type sensors were able to collect sufficient amount of charge after being irradiated to lifetime fluence expected at the HL-LHC experiment [6,7], but n-in-p sensors have a number of advantages in HEP applications:

- They do not undergo type-inversion when receiving non-ionizing bulk damage, while n-in-n type sensors do [8].
- Since the p–n junction is formed on the electrode side and the depletion zone grows from this side, charge collection is possible even without full depletion [1].
- Since the collected charge carriers are electrons, faster read-out is possible than for the p-in-n sensors. Moreover, electrons are less affected by trapping than holes [8].
- Lithography is needed on only one side, thereby lowering the manufacturing cost. This feature is vital for the application to the areas larger than 1–2 m^2 [8].

A schematic of the old-prototype sensor structure is shown in Fig. 1. Each pixel electrode is separated by inter-pixel p-stop implants. The typical size of the pixel cells is 250×50 μm^2. Sensors are connected to the FE-I4 read-out chips [9] via bump-bonding. The size of pixels on the FE-I4 is also 250×50 μm^2. Each pixel electrode is connected to virtual ground provided by the pre-amplifier when bump-bonded onto the FE-I4. SnAg or In (Ni/In) solder is used for bump-bonding. Sensors have bias structures on their surface with which I-V measurement can be done before the bump-bonding process. This prevents faulty sensors from being bump-bonded on the FE-I4s, and makes it possible to increase the overall module yield. Bias rails were also grounded and connected to each pixels via poly-Si resistors as shown in Fig. 2.

In a previous study [4], we investigated the hit and the charge collection efficiency of HPK sensors and demonstrated that both hit and charge-collection efficiency sharply dropped under the bias rail structures after irradiation with protons. The peak efficiency drop (1 – efficiency) observed was about 55% [4]. This result suggested some possible explanations for the drop in efficiency:

- Signal electrons can be drawn towards and captured in the inter-pixel region, since the surface of such region may be positively charged by the ionizing dose.
- Since the bias rail, which is connected to ground level, is just above the inter-pixel region, the electric potential in the inter-pixel region gets closer to the ground level. This further helps the electrons to be captured in the inter-pixel region. Thus, the
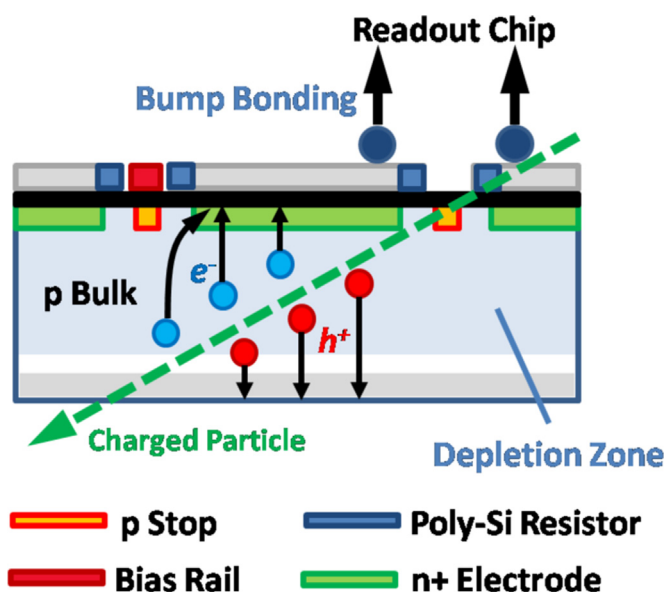

Fig. 1. A schematic of an n-in-p planar pixel sensor profile. (Old-prototype design).
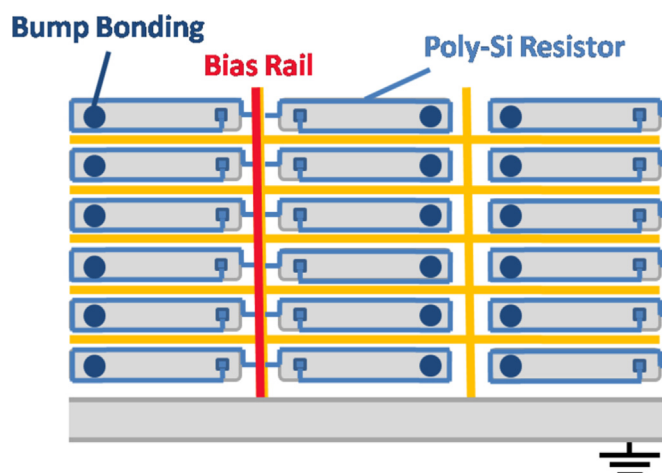

Fig. 2. A schematic view of an n-in-p planar pixel sensor from the electrode side. (Old-prototype design).

magnitude of efficiency drop is larger on the bias rail side than on the bump bonding side.

In order to minimize the loss of efficiency associated with the bias rails, several new structures have been designed based on the following ideas:

- Large offset structure: a structure which locates the bias rails on the electrodes.
- Wide p-stop structure: a structure which has broadened p-stop bands to shields the sensor bulk from the bias rails.

Furthermore, results gained from simulations conducted with a TCAD program hinted at other possible reasons for the efficiency drop [10]. The simulation triggered the investigation of sensors irradiated with γ-rays, for the purpose of decoupling the effect of surface damage from the other effects.

In order to evaluate the new sensor structures, sensor modules were irradiated with proton beams at the Cyclotron and Radio-Isotope Center (CYRIC) in Tohoku University, and with γ-rays at the Takasaki Advanced Radiation Research Institute, Japan Atomic Energy Agency (JAEA). Those irradiated modules have been tested with beams of particles (test beams) at accelerator facilities such as the Super Proton Synchrotron (SPS) at the European Organization for Nuclear Research (CERN) and DESY II at the Deutsches Elektronen-Synchrotron (DESY).

Detailed information on the devices under test (DUTs) are given in Section 2. Specific information on the proton- and γ-irradiations, followed by the details on the test beams, are presented in Section 3. The data analysis method is explained in Section 4. The analysis results are displayed in Section 5, and discussed in Section 6. Finally, conclusions are drawn in Section 7.

2. Devices under test

The modules evaluated in this analysis are listed in Table 1. The newly developed structures can be characterized by the bias rail material and the position of the bias structure. Of all the sensors investigated in this study, the wide p-stop structure is applied only on the type13. Both Al and poly-Si were used for the bias material. Each sensor structure is denoted by a sensor structure ID. The thickness of the sensor is also an important feature for evaluation, since the full-depletion voltage and the amount of collected charge

Table 1
List of evaluated samples. "ch" denotes the ROC number of four-chip modules. KEK39 and KEK93 are single-chip modules. Each ROC has 80×336 pixels.

ID	Structure ID	Bias rail material sensor structure	Thickness (μm) (sensor/ASIC)
KEK39	type10	Poly-Si rail Large offset	320/150
KEK46 ch2	type10	Poly-Si rail Large offset	150/150
KEK49 ch3	type13	Poly-Si rail Wide p-stop	150/150
KEK53 ch3	type19	No bias rail (Reference structure)	150/150
KEK71 ch3	type12	Poly-Si rail Small offset	150/150
KEK84 ch1	type2	Al rail Large offset	150/150
KEK93	type8	Al rail No offset	320/150

varies depending on the sensor thickness. Schematic views of each sensor structure are presented in Fig. 3. A detailed explanation on each sensor type can be found in a summary paper on the Japanese effort in the ITk R&D [10].

3. Irradiations and test beams

3.1. Proton irradiation at CYRIC

Proton-irradiation was carried out at CYRIC in Tohoku University. Sensor modules were aligned to make layers of DUTs in an irradiation box. Samples were exposed to 70 MeV/c proton beams up to a fluence of 3×10^{15} n_{eq}/cm^2. The hardness factor of 70 MeV protons, which was used for the conversion to 1 MeV neutron equivalent fluence, was 1.4. The beam size was evaluated by scanning the beam current with thin Al bars in the vertical and the horizontal directions. The typical resolution of the beam was $\sigma = 3 - 4$ mm of Gaussian function (Gaussian sigma). During the irradiation, the samples were cooled down to -15 °C in order to avoid annealing due to the heat generated by the beam current. Small pieces of Al foil of 1×1 cm^2 were attached on the samples for dosimetry purpose. Radiation dose was estimated after irradiation by measuring the ^{24}Na yield of Al spallation process with a Ge detector. After irradiation, all the samples were stored under -30 °C in order to mitigate the effect of annealing.

3.2. γ-ray irradiation at Takasaki

In order to replicate the expected surface damage in collider experiments, and to decouple the effect of surface damage from the other causes, a γ-ray irradiation was carried out at Takasaki. Samples were irradiated with ^{60}Co γ-source. At first, the dose rate was estimated by transmission degradation of small pieces of polymethyl methacrylate resin after three hours of radiation. The estimated dose rate was about 10 kGy/h. The irradiation lasted 10 days during which the samples received an ionizing dose of 2.4 MGy to be compared with the expected ionization dose of 7.7 MGy in the innermost layer of the ITk [5]. The samples at the proton irradiation also receive certain ionization dose. A fluence of 1×10^{16} n_{eq}/cm^2 by 70 MeV protons corresponds to 8.3 MGy from a dE/dx calculation. The effect of surface damage saturates at a specific level, and 2.4 MGy is already in the range of saturation [11].

3.3. Testbeams

The effect of radiation damage has been investigated with test beams, where a beam of particles produced by an accelerator is tracked with the help of the beam telescope. The data used in this paper were taken at the DESY II accelerator in DESY and the SPS in CERN, between 2013 and 2015.

The ACONITE telescope has six telescope planes, which are arranged behind each other in the test beam setup. These planes are realized in the form of MIMOSA26 sensors [12]. These are monolithic pixel sensors with a pixel size of 18.4×18.4 μm^2. Irradiated DUTs were installed in a cooling box located in between 3rd and 4th plane of the telescope in order to keep the DUTs at a temperature low enough to ensure equally sufficiently low leakage currents, and to minimize the effect of annealing. The typical temperature on the sensor surface was -40 °C.

A non-irradiated DUT plane was installed outside the cooling box as a reference plane. This is because the readout methods applied for the beam telescope and for FE-I4 are different: while the telescope uses the rolling-shutter method and takes 115.2 μs to complete the readout phase per trigger, the FE-I4 accumulates the
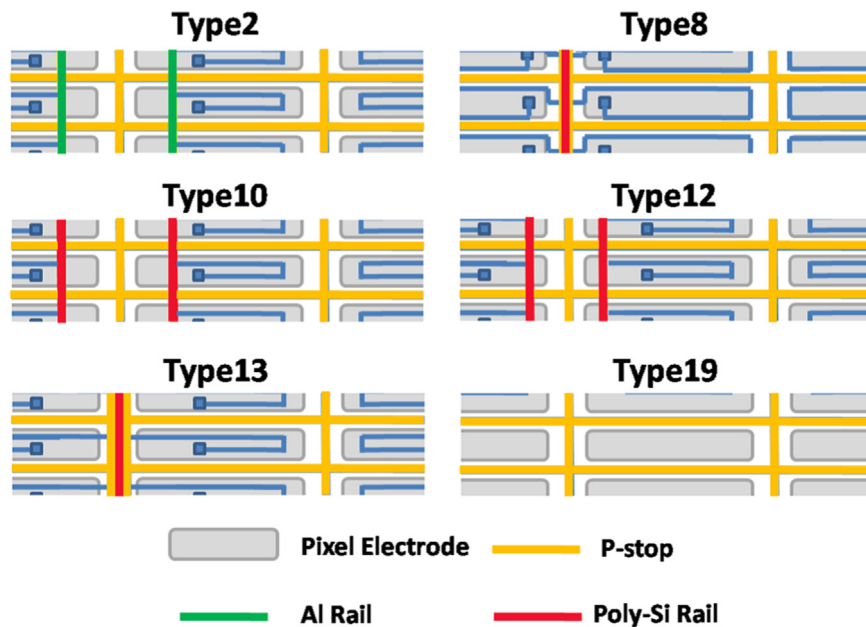
Fig. 3. Schematic views of sensor structures evaluated in this paper.

Table 2
List of proton-irradiated samples. "BC", which is the abbreviation of "bunch crossing", is a unit of ToT. 1 [BC] corresponds to 25 ns.

ID	Bias voltage (−V)	Fluence (n_{eq}/cm²)	Threshold (e) ToT (BC at ke)	Data taking period
KEK39	200, 300, 400, 500, 600, 700	4.91×10^{15}	1800 7 at 10	November 2013
KEK46 ch2	150, 200, 250, 300, 350, 400	4.18×10^{15}	1800 7 at 5	November 2013
KEK49 ch3	200, 400, 600, 800	3.20×10^{15}	1800 7 at 5	March 2014
KEK53 ch3	200, 400, 600, 800	2.35×10^{15}	1800 7 at 5	March 2014
KEK71 ch3	200, 400, 600, 800	3.08×10^{15}	2400 7 at 5	April 2015
KEK84 ch1	200, 400, 600, 800	3.03×10^{15}	3000 7 at 5	April 2015

hit information for 400 ns for every trigger. Therefore, if two or more particles pass through the test beam setup, there may be events with more than one hit on the telescope and only one hit on DUTs. In order to avoid this readout timing issue, only the tracks penetrating the reference plane are used in the analysis [13].

Proton-irradiated sensors were tested at DESY in 2013, 2014 and 2015. In 2013 and 2014, data was taken with 4 GeV/c positron beams, and in the 2015, with 4 GeV/c electron beams. The typical position resolution of tracking on the DUT planes were 26 μm in 2013 and 2014, and 30–35 μm in 2015. In order to achieve uniform performance of sensors, DUTs were calibrated before data-taking

Table 3
List of γ-irradiated sample.

ID	Bias voltage (−V)	Dose (MGy)	Threshold (e) ToT [BC at ke]	Data taking Period
KEK93	100, 200, 400	2.4	3000 7 at 10	JulY 2015

to adjust the threshold and the time-over-threshold (ToT) to deposited charge relation of each pixel to the calibration value. ToT denotes the duration of signal over threshold expressed as an unit of bunch crossing clock [9]. Data-taking was carried out under different bias voltages in order to investigate the bias voltage dependence of the detection efficiency. Table 2 lists detailed information on the tested samples.

In addition to the bulk effect, the effect of surface charge-up has been evaluated with data taken with a 120 GeV/c pion beam at the CERN SPS. The typical pointing resolution in this test beam was 8–9 μm. Details are presented in Table 3.

4. Analysis

The analysis of test beam data can be divided into two parts: Reconstruction and hit/charge-collection efficiency analysis. In the former part, particle tracks are reconstructed from hit information in raw files, exploiting the EUTelescope reconstruction framework[1] [14,15], which is realized as a couple of Marlin processors. This software makes clusters out of information of charge-collection and generates hit maps by applying geometrical information. It aligns the telescope and DUT planes at sub-micron level, so as to build final tracks with good precision. Finally, it builds the final tracks and generates the track data-collection.

In the latter part of analysis, an offline analysis framework TBmon2[2] is used. This software loads the output file from the EUTelescope package and, making use of its track information, calculates the detection efficiency of DUTs. Only tracks which pass through the reference plane are used. Hit efficiency is defined as the ratio of the number of tracks associated with hits within certain radius to the total number of tracks. The track-hit finding radius (match width) varies depending on the pointing resolution. Evaluation of the hit efficiency is carried out at two different levels: overall hit efficiency and sub-pixel resolved hit efficiency. Overall hit efficiency is displayed in the granularity of the sensor size, while the sub-pixel resolved hit efficiency visualizes the
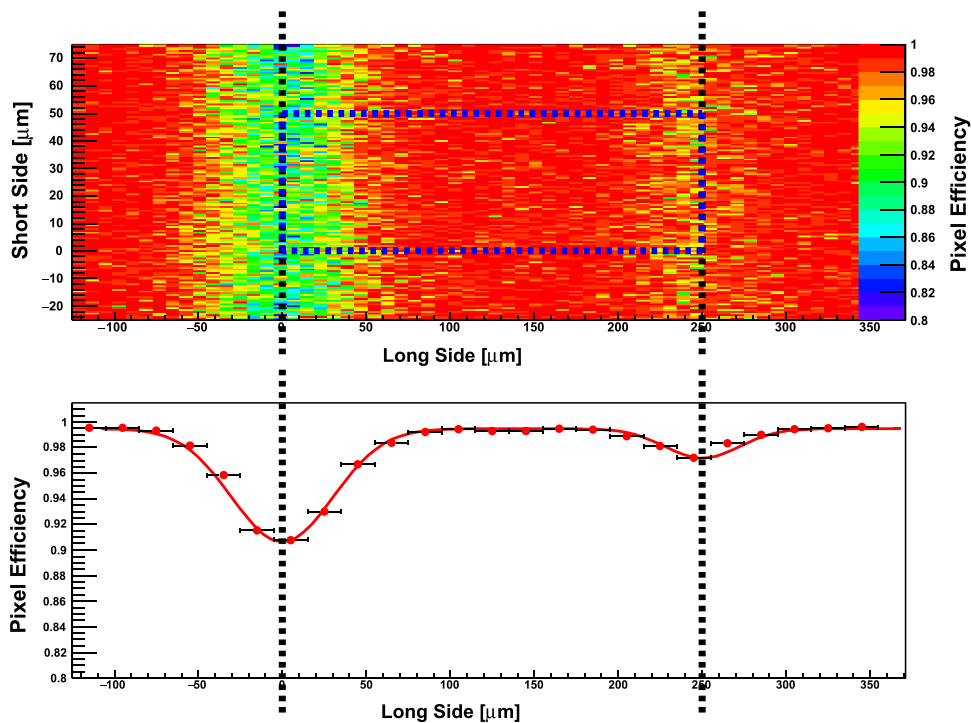
Fig. 4. A sub-pixel resolved efficiency map (upper part) and a projected pixel efficiency map (lower part) created from KEK71 ch3 (−800 V) data. The rectangle drawn in the sub-pixel resolved efficiency map indicates the area of one pixel.

contrast in efficiency among different pixel structures. In order to investigate the effect of pixel structures, the pixel efficiency map is produced as shown in the upper part of Fig. 4. The area displayed in the pixel efficiency map corresponds to 2×2 pixel-size. This pixel map shows the sub-pixel resolved efficiency in $1 \times 1~\mu m^2$ resolution.

The bottom part of Fig. 4 presents the projected efficiency along the X-direction. This projection map is created by dividing the projected hit map with the projected track map. The efficiency in the electrode region is defined as the offset value of double-Gaussian plus offset fit function.

In order to evaluate the efficiency drop quantitatively, a numerical value, efficiency loss per pixel ε_{loss}^{reg} is introduced as follows:

$$\varepsilon_{loss}^{reg} = \frac{S_{loss}}{L^{reg} \times \alpha_{eff}^{Electrode}} \tag{1}$$

This value is calculated from the projected pixel efficiency map. First, the area of each Gaussian function is calculated in order to obtain the total amount of efficiency drop S_{loss} along the X-direction. Second, the calculated area of Gaussian function is divided by two-pixel length L^{reg} to uniformly average the inefficiency in 2×2 pixel map. Finally, the averaged value is normalized with the efficiency in the electrode region $\alpha_{eff}^{Electrode}$. This value represents averaged ratio of "the total inefficiency in each pixel boundary" to "the hit efficiency in the electrode region". Hence, the name, "efficiency loss per pixel". The inefficiencies of each sensor structure are compared in the next section exploiting this analysis method [16].

5. Results

5.1. Proton-irradiated modules

The dependency of the overall efficiency on the bias voltage is presented in Fig. 5. The data used in this plot is from test beams in
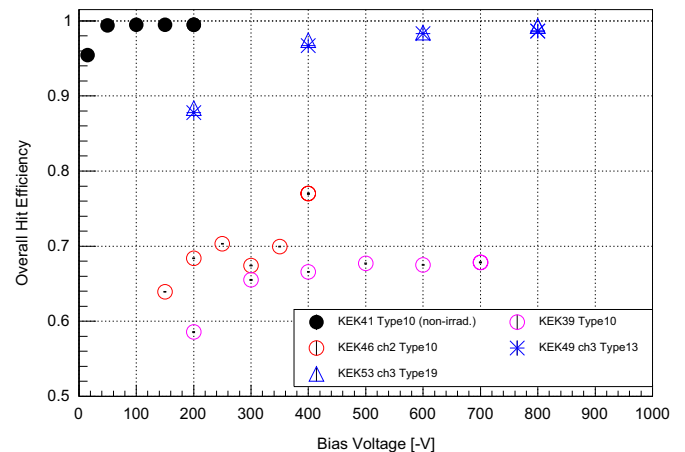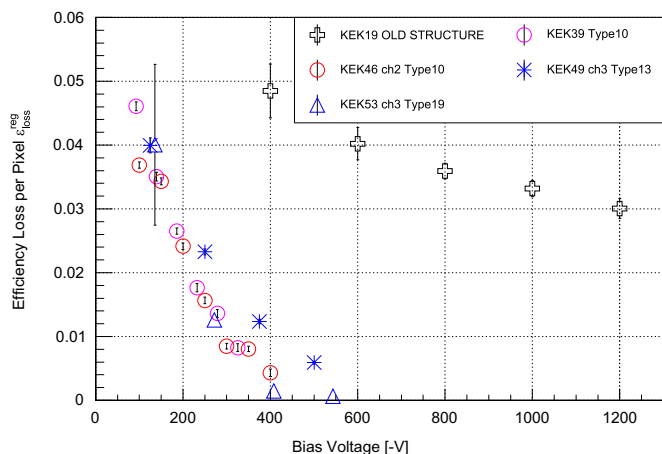

Fig. 5. Bias voltage dependence of overall hit efficiency of DUTs in DESY test beams held in 2013 and 2014 [16]. The filled black dot represents a non-irradiated reference sensor, KEK41.

2013 and 2014. KEK41 is a Type10 sensor installed as a non-irradiated reference, which achieved an efficiency of $99.481 \pm 0.009\%$ at -200 V. The overall efficiency of KEK49 ch3 and KEK53 ch3 reached $98.620 \pm 0.024\%$ and $99.320 \pm 0.066\%$ respectively at -800 V. The errors are calculated making use of the Bayesian statistics.

Since there was no reference plane installed in the November 2013 test beam, the overall efficiencies of KEK39 and KEK46 ch2 are $67.831 \pm 0.049\%$ (-700 V) and $76.992 \pm 0.051\%$ (-400 V) respectively, which are lower than that of the other sensors [16].

The efficiency loss per pixel of those sensors is calculated with the method introduced in Section 4, and Fig. 6 displays its bias voltage dependency. However, since the thickness and the radiation fluence of the samples differ, it is not possible to directly compare the efficiency loss. The plots in Fig. 6 were scaled by using the efficiency loss on the bump-bonding side, since all sensor

Fig. 6. Bias voltage dependency of efficiency loss per pixel of DUTs in DESY test beams held in 2013 and 2014 [16].
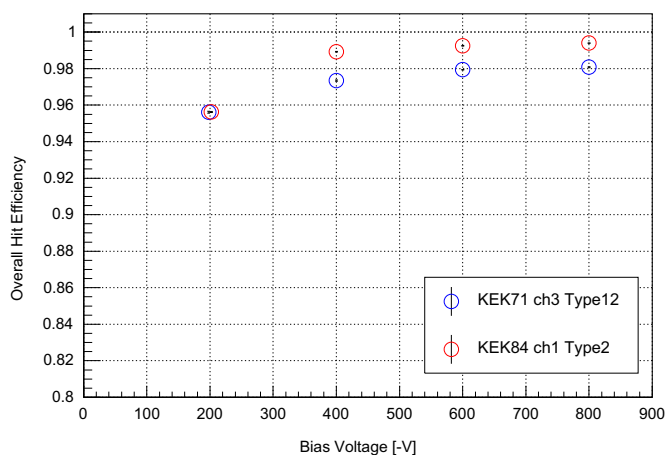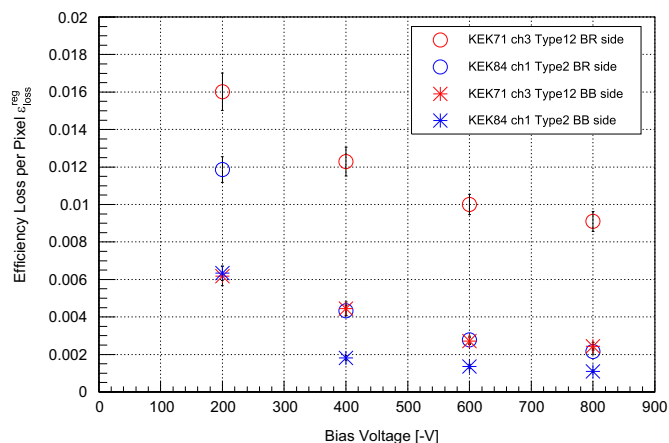

Fig. 7. Bias voltage dependency of overall hit efficiency of DUTs in DESY test beams held in 2015.

Fig. 8. Bias voltage dependency of efficiency loss per pixel of DUTs in DESY test beams held in 2015. The efficiency loss per pixel in the bump bonding side (denoted by BB side) and bias rail side (denoted by BR side) is displayed separately.

Fig. 9. Bias voltage dependency of efficiency loss per pixel of γ-irradiated KEK93 in CERN test beam held in 2015. The red plot represents KEK93 and the blue plots represents proton-irradiated KEK84 ch1. (For interpretation of the references to color in this figure caption, the reader is referred to the web version of this paper.)
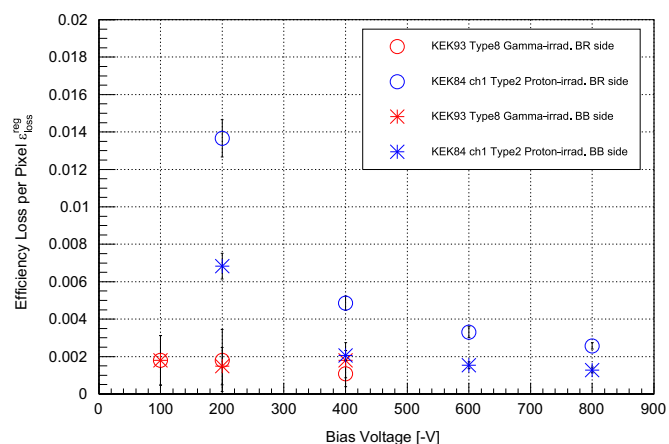
types have the identical geometry on that side, and the efficiency should be the same if the thickness and the fluence are the same. In order to scale the plots, the inefficiency loss versus bias voltage plot in the bump-bonding side was fitted with complementary error function $1 - \mathrm{Erf}$, since the efficiency as a function of bias voltage should follow the integrated Gauss distribution when the bias voltage is sufficiently high. Then, the fit function for each sensor is scaled to reproduce the shape of reference plots so as to get scaling factors. Finally, those scaling factors are applied to the bias rail side. In Fig. 6, KEK46 ch2 is used as a reference point.

The KEK19 module in Fig. 6 has the old type sensor structure, a structure with neither a bias rail offset nor a wide p-stop. The thickness of KEK19 is 150 μm. This old-type module was irradiated up to $5.0 \times 10^{15}\, n_{\mathrm{eq}}/\mathrm{cm}^2$ and was tested in the March 2013 test beam at DESY. Comparison with the old-type structure and the new structures is made in Section 6.1.

The overall efficiency of the other proton-irradiated sensors is displayed in Fig. 7. Since at least one reference plane was installed in the test beam at DESY 2015, the overall efficiency reached over 95% at -800 V. KEK71 ch3, however, presents relatively lower overall efficiency, even if the bias voltage is high enough for the 150 μm-thick sensors to be fully depleted. A possible reason for this is that the ToT distribution of KEK71 ch3 is much broader than usual, and there could be a finite number of events that were lower in charge than the threshold value. In addition, the peak ToT value of KEK71 ch3 is lower than that of KEK84 ch1, which indicates the relative threshold for the KEK71 ch3 is higher than that for KEK84 ch1.

The efficiency loss per pixel of KEK71 ch3 and KEK84 ch1 is shown in Fig. 8. Unlike Fig. 6, the efficiency loss per pixel in the bump bonding side and the bias rail side is calculated and displayed separately. A comparison between large and small offset structures is possible from this figure, and this is discussed in detail in Section 6.2.

5.2. γ-irradiated modules

Bias voltage dependence of the efficiency loss per pixel of KEK93 is presented in Fig. 9. The red plots represents the γ-irradiated KEK93. In order to compare the efficiency drop with a bulk-damaged module, proton irradiated data of KEK84 ch1 is shown as the blue plots. One important point on this figure is that these plots are not scaled even though the sensor thickness differs between KEK93 (320 μm) and KEK84 ch1 (150 μm). A detailed discussion can be found in Section 6.3.

6. Discussion

6.1. Comparison between new and old structures

Fig. 6 indicates that the efficiency of new sensor structures is significantly improved compared with the old structures. Since the

fluence and the thickness of the sensors differed among the tested samples, scaling was done as explained in 5.1. The ideas of large offset and wide p-stop structures are considered effective in improving detector performance after irradiation. The amount of efficiency loss differs among the new structures. If they are lined up in descending order of efficiency drop, the order is as follows: type13, type10, type19. In particular, type10, which has a large offset structure, shows almost equivalent efficiency loss to type19, which does not have a bias rail structure. This indicates that the large offset structure is close to the ideal case, because no-bias rail structure should not be affected by the efficiency drop caused by bias structure.

6.2. Comparison between large and small structures

Fig. 8 indicates that the large offset structure presents the smaller amount of efficiency loss. The difference is especially prominent on the bias rail side. This is reasonable because the sensor structure is the same on the bump bonding side. Putting together the results in Fig. 6, the large offset structure can be considered as a strong candidate for the final detector design. This analysis, however, has been done with different bias rail materials: KEK84 ch1 with Al rail and KEK71 ch3 with poly-Si rail. Thus, further comparison between different material is still necessary to decide on the final design.

6.3. Effect of surface damage

Fig. 9 points out that the efficiency loss of the γ-irradiated sensor is only less than 0.5%. Still, as described in Section 5.2, the sensors compared in Fig. 9 have different thickness, and scaling is necessary to compare the result quantitatively. However, the effect of sensor thickness enlarges the difference in the efficiency loss: if the samples had the same thickness, 320 μm for the proton-irradiated sample for instance, the plots of proton-irradiated sensor in Fig. 9 would shift towards the higher voltage direction. The effect of surface damage is caused by the Si–SiO2 interface-charge. The charge density in the interface region increases as the ionization dose grows, and is known to be saturated when the amount of ionization dose reaches the order of MGy [17]. This means that the harshest surface damage was replicated by 2.4 MGy of radiation dose. For that reason, it is clear that the efficiency loss in the γ-irradiated sensor is remarkably small compared with the proton-irradiated sensors. Thus, the effect of surface charge-up can be considered as notably smaller than that of bulk damage.

7. Conclusions

New sensor structures which are developed based on the indication from the previous study were evaluated at test beams at DESY and CERN. Data from the test beams in 2013 and 2014 indicated that new sensor structures achieved significantly smaller efficiency loss compared with the old type sensors. Especially, the large offset structure achieved almost the same level of efficiency loss as no bias rail structure, which was expected to show the least efficiency loss. Furthermore, a comparison between the large offset structure and the small offset structure indicated that the larger offset structure presented better detection efficiency. Further comparison between Al and poly-Si bias rail structure is still necessary to complete the optimization of the new sensor structure. In addition, an investigation of the effect of Oxide-Si interface charge-up, which had been indicated by a TCAD analysis [10], was carried out in order to decouple the effect of surface charge-up from that of bulk damage. Data taken with a sensor irradiated with γ-ray presented that the efficiency loss on the γ-irradiated sensor is remarkably small compared with proton-irradiated sensors. This indicated that the surface charge-up was not a contributory factor to the efficiency drop.

References

[1] S. Kamada, et al., Development of N+ in P pixel sensors for a high luminosity large hadron collider, Nucl. Instrum. Methods Phys. Res. Sect. A 765 (2014) 118–124.

[2] Y. Unno, et al., Development of novel n+-in-p silicon planar pixel sensors for HL-LHC, Nucl. Instrum. Methods Phys. Res. Sect. A 699 (2013) 72–77.

[3] R. Nagai, et al., Evaluation of novel KEK/HPK n-in-p pixel sensors for ATLAS upgrade with testbeam, Nucl. Instrum. Methods Phys. Res. Sect. A 699 (2013) 78–83.

[4] K. Motohashi, et al., Evaluation of KEK n-in-p planar pixel sensor structures for very high radiation environments with testbeams, Nucl. Instrum. Methods Phys. Res. Sect. A 765 (2014) 125–129.

[5] ATLAS collaboration, ATLAS Letter of Intent Phase-II Upgrade, Techical Report CERN-2012-022 LHCC-I-023, CERN, 2012.

[6] J. Weingarten, et al., Planar pixel sensors for the atlas upgrade: beam tests results, J. Instrum. 7 (10) (2012) P10028.

[7] A. Rummler, Investigation of radiation damage in n+-in-n planar pixel sensors for future ATLAS pixel detector upgrades (Ph.D. thesis), TU Dortmund, 2014.

[8] L. Rossi, P. Fischer, T. Rohe, N. Wermes, Pixel Detectors, Springer, Berlin Heidelberg, 2012.

[9] FE-I4 Collaboration, The FE-I4B Integrated Circuit Guide Version 2.3 (2012).

[10] Y. Unno, et al., Development of n+-in-p planar pixel sensors for very high radiation environments, designed to retain high efficiency after irradiation, Nucl. Instrum. Methods Phys. Res. Sect. A, this issue.

[11] K.A. Olive, et al., Review of Particle Physics, Chin. Phys. C38 (2014) 090001, http://dx.doi.org/10.1088/1674-1137/38/9/090001.

[12] C. Hu-Guo, et al., A ten thousand frames per second readout MAPS for the EUDET beam telescope, Topical Workshop on Electronics for Particle Physics, 2009, pp. 47–51.

[13] J. Weingarten, et al., Planar pixel sensors for the ATLAS upgrade: beam tests results, J. Instrum. 7 (2012) 28.

[14] I. Rubinskiy, EUTelescope. Offline Track Reconstruction and DUT Analysis Software, Techical Report, 2010.

[15] H. Perrey, EUDAQ and EUTelescope – Software Frameworks for Testbeam Data Acquisition and Analysis.

[16] D. Yamaguchi, Beamtests of HPK/KEK n+-in-p pixel sensors for ATLAS HL-LHC upgrade inner tracker, 10th Anniversary "Trento" Workshop on Advanced Silicon Radiation Detectors, Trento (Italy), 17–19 Feb 2015, 2015. ⟨https://bib-pubdb1.desy.de/record/292089⟩.

[17] J. Zhang, E. Fretwurst, R. Klanner, I. Pintilie, J. Schwandt, M. Turcato, Investigation of x-ray induced radiation damage at the Si–Sio2 interface of silicon sensors for the European xfel, J. Instrum. 7 (12) (2012) C12012 ⟨http://stacks.iop.org/1748-0221/7/i=12/a=C12012⟩.